


Double-Transmon Coupler: Fast Two-Qubit Gate with No Residual Coupling for Highly Detuned Superconducting Qubits

Hayato Goto^{✉*}

Frontier Research Laboratory, Corporate Research & Development Center, Toshiba Corporation, 1, Komukai
Toshiba-cho, Saiwai-ku, Kawasaki-shi 212-8582, Japan

 (Received 21 March 2022; revised 25 July 2022; accepted 28 July 2022; published 15 September 2022)

Although two-qubit entangling gates are necessary for universal quantum computing, they are notoriously difficult to implement with high fidelity. Recently, tunable couplers have become a key component for realizing high-fidelity two-qubit gates in superconducting quantum computers. However, it is still difficult to achieve tunable coupling free of unwanted residual coupling—in particular, for highly detuned qubits, which are desirable for mitigating qubit-frequency crowding or errors due to crosstalk between qubits. We thus propose a kind of tunable coupler that we call a double-transmon coupler, because it is composed of two transmon qubits coupled through a common loop with an additional Josephson junction. By controlling the magnetic flux in the loop, we can achieve not only fast high-fidelity two-qubit gates but also no residual coupling during the idle time, where computational qubits are highly detuned fixed-frequency transmons. The proposed coupler is expected to offer an alternative approach to higher-performance superconducting quantum computers.

DOI: [10.1103/PhysRevApplied.18.034038](https://doi.org/10.1103/PhysRevApplied.18.034038)

I. INTRODUCTION

Remarkable advances have been made in the technologies for realizing quantum computers over the past decade. Nevertheless, two-qubit entangling gates, which are necessary for universal quantum computing together with single-qubit gates [1–7], are still hard to implement with high fidelity. For instance, two-qubit gates with a fidelity of over 99%, which is necessary for tasks such as fault-tolerant quantum computation using quantum error correction [8–12], have been demonstrated experimentally by using only a few kinds of physical systems: laser-cooled trapped ions [13–18], superconducting circuits [19–32], and, most recently, silicon-based approaches such as quantum dots [33–35] and donor spins [36]. Among these, superconducting circuits may be promising in the sense that their qubits are, of course, solid-state devices and therefore do not need trapping, unlike trapped ions, and also two-dimensional qubit arrays have already been realized [21,24,37], which is still difficult for quantum dots, by recently developed three-dimensional integration technologies [38–40].

Tunable couplers have recently become a key component for high-fidelity two-qubit gates in superconducting quantum computers [21–24,27–29,32,41–48]. Tunable couplers allow us not only to implement fast two-qubit gates but also to turn off an energy-exchange interaction called transverse or XY coupling [49]. Major tunable couplers, including those used for demonstration of quantum supremacy (advantage) [21,24], are based on the cancellation between a direct coupling via a capacitor and an indirect coupling via a frequency-tunable transmon qubit [50], which we refer to as a single-transmon coupler. This coupler is regarded as a capacitor or transmon version of a previously proposed inductor-based coupler for flux qubits [51,52]. (Other kinds of inductor-based tunable couplers have also been proposed [53–56].) In the single-transmon coupler, there exists an unwanted correlated energy shift due to residual coupling called longitudinal or ZZ coupling [49]. Residual ZZ coupling has recently become a central issue in the field of superconducting quantum computers [23,27–32,41–46,57–63]. Some research groups have found special conditions under which the ZZ coupling in the single-transmon coupler vanishes [28,42]. However, the vanishing points exist only in a region of small detunings between two computational qubits [28] (see Appendix E). In other words, in the single-transmon coupler, there is inevitable ZZ coupling for highly detuned qubits [23,43]. Thus, zero ZZ coupling in the single-transmon coupler results in qubit-frequency crowding or crosstalk between qubits [64].

*hayato1.goto@toshiba.co.jp

Published by the American Physical Society under the terms of the [Creative Commons Attribution 4.0 International](https://creativecommons.org/licenses/by/4.0/) license. Further distribution of this work must maintain attribution to the author(s) and the published article's title, journal citation, and DOI.

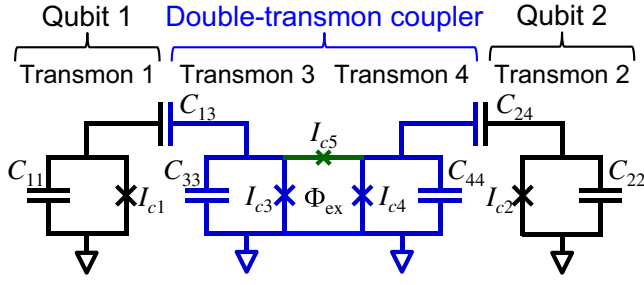


FIG. 1. A diagram of the proposed double-transmon coupler with two computational qubits. Parasitic capacitances are considered in this work but are not shown for simplicity.

In this paper, we theoretically propose a tunable coupler that we call a double-transmon coupler. Our coupler consists of two fixed-frequency transmons coupled through a common loop with an additional Josephson junction. We can control the coupling between the two coupler transmons by controlling the magnetic flux in the loop and consequently we tune the coupling strength between computational qubits. A notable feature of this coupler is that the ZZ coupling vanishes even for highly detuned computational qubits, unlike the single-transmon coupler. Our numerical simulations indicate that this coupler allows us to achieve not only high two-qubit gate fidelities of over 99.99% with a short gate time of 24 ns but also no residual ZZ coupling during the idle time for highly detuned fixed-frequency transmons with a detuning of 0.7 GHz. Thus, the double-transmon coupler is expected to be promising for improving the performance of superconducting quantum computers.

II. DESIGN AND MECHANISM

Figure 1 shows a diagram of the proposed coupler. This consists of two fixed-frequency transmons (transmons 3 and 4 in Fig. 1) coupled through a common loop with an additional Josephson junction, the critical current of which is smaller than that of the transmons. Two computational

qubits (transmons 1 and 2 in Fig. 1) are capacitively coupled to the coupler, as shown in Fig. 1.

The mechanism of this coupler is qualitatively explained from a classical point of view under rough approximations as follows [65]. The Lagrangian describing the total system is given by $L = K - V$, with

$$K = \sum_{i=1}^4 \frac{C_{ii}}{2} \dot{\phi}_i^2 + \sum_{i=1}^2 \sum_{j=i+1}^4 \frac{C_{ij}}{2} (\dot{\phi}_i - \dot{\phi}_j)^2 + \frac{C_{34}}{2} \dot{\phi}_5^2, \quad (1)$$

$$V = - \sum_{i=1}^5 \hbar \omega_{Ji} \cos \phi_i, \quad (2)$$

where ϕ_i , $\dot{\phi}_i = \phi_0 \dot{\phi}_i$, and $\hbar \omega_{Ji} = \phi_0 I_{ci}$ are, respectively, the phase difference, the flux variable, and the Josephson energy for the i th Josephson junction with a critical current of I_{ci} [66], the dots denote time derivatives, and we include unwanted parasitic capacitances.

Neglecting the parasitic capacitances and using the constraint that $\phi_5 = \phi_4 - \phi_3 - \Phi_{\text{ex}}$ (Φ_{ex} is the external flux in the loop) [67], we can approximate K and V as

$$K \approx \sum_{i=1}^4 \frac{C_{ii}}{2} \dot{\phi}_i^2 + \frac{C_{13}}{2} (\dot{\phi}_1 - \dot{\phi}_3)^2 + \frac{C_{24}}{2} (\dot{\phi}_2 - \dot{\phi}_4)^2, \quad (3)$$

$$V \approx - \sum_{i=1}^4 \hbar \omega_{Ji} \cos \phi_i - \hbar \omega_{J5} \cos(\phi_4 - \phi_3 - \Theta_{\text{ex}}), \quad (4)$$

where $\Theta_{\text{ex}} = \Phi_{\text{ex}}/\phi_0$. Note that the two qubits are coupled only through the coupling between the two coupler transmons given by the last term in Eq. (4). This coupling can approximately be turned off by tuning the external flux Φ_{ex} , as follows.

Here, we focus on the potential for the coupler V_c . In the transmon regime, where the Josephson energies are much larger than the charging energies [68], low-energy states concentrate around a potential minimum and hence the following second-order approximation is valid:

$$\begin{aligned} V_c &= -\hbar \omega_{J3} \cos \phi_3 - \hbar \omega_{J4} \cos \phi_4 - \hbar \omega_{J5} \cos(\phi_4 - \phi_3 - \Theta_{\text{ex}}) \\ &\approx \frac{\hbar}{2} \begin{pmatrix} \delta_3 & \delta_4 \end{pmatrix} \begin{pmatrix} \omega_{J3} \cos \phi_3^{(0)} + \omega_{J5} \cos(\phi_4^{(0)} - \phi_3^{(0)} - \Theta_{\text{ex}}) & -\omega_{J5} \cos(\phi_4^{(0)} - \phi_3^{(0)} - \Theta_{\text{ex}}) \\ -\omega_{J5} \cos(\phi_4^{(0)} - \phi_3^{(0)} - \Theta_{\text{ex}}) & \omega_{J4} \cos \phi_4^{(0)} + \omega_{J5} \cos(\phi_4^{(0)} - \phi_3^{(0)} - \Theta_{\text{ex}}) \end{pmatrix} \begin{pmatrix} \delta_3 \\ \delta_4 \end{pmatrix}, \end{aligned} \quad (5)$$

where $\phi_3^{(0)}$ and $\phi_4^{(0)}$ are the phase differences minimizing V_c , $\delta_i = \phi_i - \phi_i^{(0)}$, and constants have been dropped. Note that when Θ_{ex} is equal to $\Theta_{\text{ex}}^{(0)}$, satisfying $\cos(\phi_4^{(0)} - \phi_3^{(0)} - \Theta_{\text{ex}}^{(0)}) = 0$, the nondiagonal elements of

the matrix in Eq. (5) vanish, and consequently the coupling between the two coupler transmons is turned off, as desired. This mechanism is substantially different from that of the single-transmon coupler [64].

III. ZZ COUPLING

In order to accurately evaluate the properties of the double-transmon coupler, here we numerically investigate it using a fully quantum mechanical model with finite parasitic capacitances. In this work, the qubits are assumed to be detuned. The qubit states are then well defined by the energy eigenstates of the total Hamiltonian. However, there can be an unwanted correlated energy shift due to residual ZZ coupling. The ZZ coupling strength ζ_{ZZ} is defined as

$$\zeta_{ZZ} = \omega_{11} - (\omega_{10} + \omega_{01}), \quad (6)$$

where $\omega_{ij} = E_{ij}/\hbar$ is the frequency corresponding to the energy, E_{ij} , of the two-qubit state $|ij\rangle$. We also set the origin of energy as $\omega_{00} = 0$. When $\zeta_{ZZ} = 0$, the two qubits are completely independent.

By numerically diagonalizing the quantum mechanical Hamiltonian derived from the Lagrangian given by Eqs. (1) and (2) (see Appendix A), we evaluate ζ_{ZZ} for two situations: larger and smaller detunings between the qubits than the anharmonicities (Kerr coefficients) of the qubits, which are, respectively, called “out of the straddling regime” and “in the straddling regime.” The results in the two situations are, respectively, shown in Figs. 2(a) and 2(b), where the parameters are set to experimentally feasible values [43]. From these results, it turns out that the double-transmon coupler can have the vanishing points of the ZZ coupling in both the regimes. This is a notable feature of the double-transmon coupler, because for the conventional single-transmon coupler, the ZZ-coupling vanishing points exist only in the straddling regime [28] (see Appendix E). It is also interesting that the coupler-transmon frequency required for the zero ZZ coupling is lower bounded out of the straddling regime but upper bounded in the straddling regime [69].

IV. TWO-QUBIT GATE

We evaluate the two-qubit gate performance by numerical simulations with the parameter values in Fig. 2(a) and $\omega_4/(2\pi) = 8.5$ GHz [indicated by the horizontal dashed line in Fig. 2(a)] [70]. The Θ_{ex} dependence of ζ_{ZZ} for these parameter values is shown in Fig. 3(a). As shown in the inset, the ZZ coupling vanishes at $\Theta_{\text{ex}} \simeq 0.61\pi$ and 0.63π . We thus define the qubit states by the energy eigenstates at $\Theta_{\text{ex}} = 0.61\pi$. In other words, we set $\Theta_{\text{ex}} = 0.61\pi$ during the idle time, as indicated in Fig. 3(a).

In Fig. 3(a), it is also notable that $|\zeta_{ZZ}|/(2\pi)$ becomes as large as 40 MHz at $\Theta_{\text{ex}} = \pi$. This property can be used for a fast two-qubit gate called the controlled-phase (CPHASE) gate, including the controlled-Z (CZ) gate [23,28,43], where ζ_{ZZ} is adiabatically increased and then decreased by controlling the external flux Φ_{ex} . The flux pulse shape in the present simulations is shown in Fig. 3(b), which is

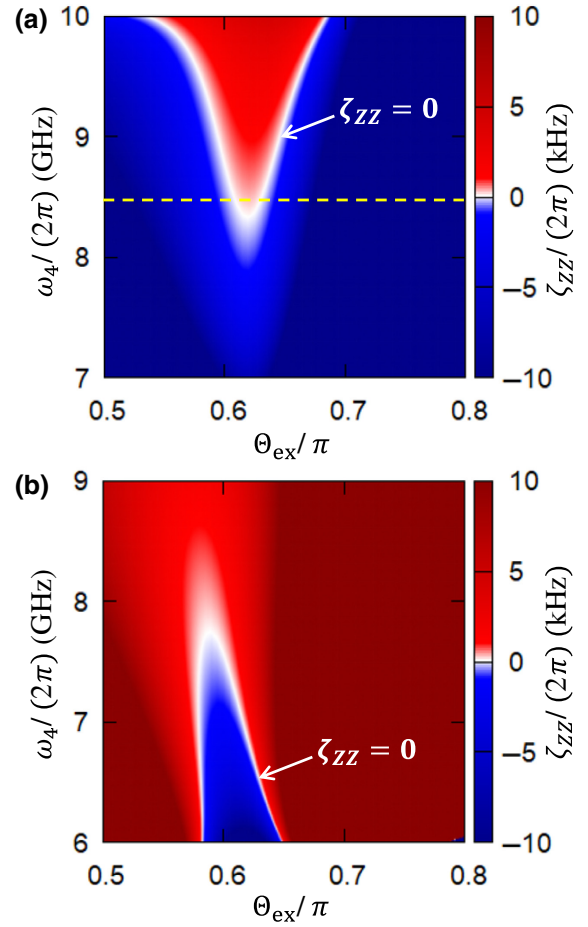


FIG. 2. The ZZ-coupling strength ζ_{ZZ} in the double-transmon coupler as a function of Θ_{ex} and the design value of the transmon-4 frequency denoted by ω_4 . The design values of the other transmon frequencies are set as $\omega_1/(2\pi) = 5$ GHz, $\omega_2/(2\pi) = 5.7$ GHz (a) or 5.1 GHz (b), and $\omega_3/(2\pi) = 7.2$ GHz. The detuning between the qubits is thus about 0.7 GHz in (a) and 0.1 GHz in (b). The capacitances are set as $C_{11} = C_{22} = C_{33} = C_{44} = 60$ fF, $C_{13} = C_{24} = 6$ fF, $C_{34} = 1$ fF, and $C_{14} = C_{23} = 2C_{12} = 0.05$ fF. The resultant anharmonicities of the four transmons are about 0.3 GHz (see Appendix D). Thus, (a) is out of the straddling regime and (b) is in the straddling regime. The horizontal dashed line in (a) [$\omega_4/(2\pi) = 8.5$ GHz] indicates the situation for the two-qubit gate simulations presented in Fig. 3.

designed according to a technique for reducing nonadiabatic errors [71] (see Appendix C). The simulation results are shown in Figs. 3(c) and 3(d).

Figure 3(c) shows that the rotation angle, θ_{CPHASE} , of the CPHASE gate increases linearly as the gate time T_g increases. The CZ gate corresponding to $\theta_{\text{CPHASE}} = \pi$ can be achieved when $T_g \simeq 24$ ns, as indicated by the horizontal dashed line in Fig. 3(c). The average fidelity of the CPHASE gate is shown in Fig. 3(d) (see Appendix B), suggesting that the CZ-gate fidelity, indicated by the vertical dashed line in Fig. 3(d), will surpass 99.99%. Thus, the double-transmon coupler allows us to simultaneously

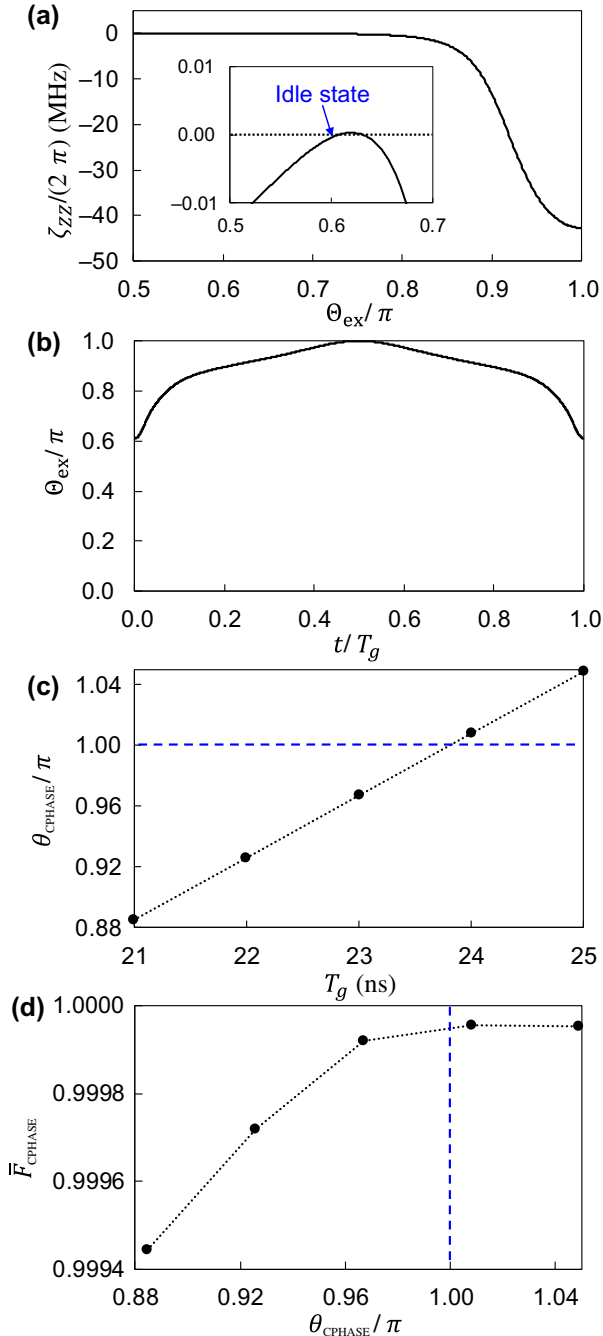


FIG. 3. The two-qubit gate with the double-transmon coupler. (a) ZZ-coupling strength ζ_{ZZ} on the dashed line in Fig. 2(a) [$\omega_4/(2\pi) = 8.5$ GHz]. The inset is an enlarged view around the ZZ-coupling vanishing points. (b) The flux pulse shape for the CPHASE gate (T_g is the gate time). (c) The rotation angle θ_{CPHASE} of the CPHASE gate with a gate time of T_g . (d) The average CPHASE-gate fidelity \bar{F}_{CPHASE} corresponding to θ_{CPHASE} . In (c) and (d), the dashed lines indicate $\theta_{\text{CPHASE}} = \pi$, corresponding to the CZ gate.

achieve fast high-fidelity two-qubit gates and no residual coupling during the idle time for highly detuned qubits [72]. The infidelity is mainly due to leakage errors caused

by nonadiabatic transitions from $|01\rangle$ and $|11\rangle$ to higher levels outside the qubit subspace (see Appendix C). For instance, when the gate time is 24 ns, 20% and 73% of the average infidelity are due to the leakage errors from $|01\rangle$ and $|11\rangle$, respectively.

V. FLUX NOISE

Although the qubits are fixed-frequency transmons, the qubit frequencies vary a little depending on the flux in the coupler (see Appendix A). Here, we examine the influence of the flux noise on the qubit coherence.

The coherence time T_2 for qubit 1 in terms of the flux noise is formulated as [68]

$$T_2 \approx \left| A_\Phi \frac{\partial \omega_{10}}{\partial \Phi_{\text{ex}}} \right|^{-1} = \left| 2\pi \frac{A_\Phi}{\Phi_0} \frac{\partial \omega_{10}}{\partial \Theta_{\text{ex}}} \right|^{-1}, \quad (7)$$

where the coefficient A_Φ is typically $10^{-5}\Phi_0$ [66,68] (T_2 for qubit 2 is given similarly). Using the parameter values in Fig. 3 and $A_\Phi = 10^{-5}\Phi_0$, the T_2 values for qubits 1 and 2 are numerically estimated to be about 260 μs and 430 μs , respectively, in the idle state. These long coherence times suggest the robustness of the proposed scheme against flux noise.

During the two-qubit gate, Θ_{ex} changes from 0.61π to π . In this range of Θ_{ex} , the minimum values of T_2 estimated as above are 30 μs and 5 μs , respectively, for qubits 1 and 2. Even in the worst-case scenario where the coherence time is assumed to be 5 μs , the infidelity of the CPHASE gate with a gate time of 24 ns may increase to about 0.5%, which is still small. This rough estimation suggests that the flux noise may not degrade the gate performance very much.

VI. CONCLUSIONS

We theoretically propose a tunable coupler for superconducting quantum computers. We call this a double-transmon coupler, because it consists of two fixed-frequency transmons coupled through a common loop with an additional Josephson junction. We find numerically that by tuning the external flux in the loop, residual ZZ coupling vanishes even for highly detuned computational qubits, in contrast to the conventional single-transmon coupler. The numerical simulations also show that the proposed coupler enables two-qubit gates with a high fidelity of over 99.99% and a short gate time of 24 ns. The next step is experimental realization of this proposal, where relaxation and decoherence in transmons will degrade the performance. However, from its short gate time (24 ns) and the recently reported long coherence times of transmons (over 300 μs) [73,74], the proposed coupler is expected to achieve high two-qubit gate fidelity. Another important issue in experiments is the unwanted deviation of critical currents of Josephson junctions from design values. The precision of

the critical currents is known to be about 2%, though this can be reduced by laser annealing [75]. The effects of the critical-current deviation on the coupler performance are left as an important issue for future work.

APPENDIX A: QUANTUM MECHANICAL MODEL

Using the constraint that $\phi_5 = \phi_4 - \phi_3 - \Phi_{\text{ex}}$, the kinetic energy term in Eq. (1) can be expressed as

$$K = \frac{1}{2} \dot{\boldsymbol{\phi}}^T M \dot{\boldsymbol{\phi}} - \mathbf{q}^T \dot{\boldsymbol{\phi}}, \quad (\text{A1})$$

where $\dot{\boldsymbol{\phi}}^T = (\dot{\phi}_1 \ \dot{\phi}_2 \ \dot{\phi}_3 \ \dot{\phi}_4)$, $\mathbf{q}^T = (0 \ 0 \ -C_{34} \dot{\Phi}_{\text{ex}} C_{34} \dot{\Phi}_{\text{ex}})$, and M is a capacitor matrix. The canonical conjugate variables for the flux variables, namely, the charge variables \mathbf{Q} , and the Hamiltonian are obtained as

$$\mathbf{Q} = \frac{\partial L}{\partial \dot{\boldsymbol{\phi}}} = M \dot{\boldsymbol{\phi}} - \mathbf{q}, \quad (\text{A2})$$

$$H = \mathbf{Q}^T \dot{\boldsymbol{\phi}} - L = \frac{1}{2} \mathbf{Q}^T M^{-1} \mathbf{Q} + \mathbf{q}^T M^{-1} \mathbf{Q} + V. \quad (\text{A3})$$

Introducing the Cooper-pair number variables as $\mathbf{n} = \mathbf{Q}/(2e)$ (where e is the elementary charge), H is rewritten as

$$H = 4\hbar \mathbf{n}^T W \mathbf{n} + \hbar \frac{\dot{\Phi}_{\text{ex}}}{\omega_{C34}} (00 - 11) W \mathbf{n} + V, \quad (\text{A4})$$

where $\hbar W = e^2/2M^{-1}$ and $\hbar\omega_{C34} = e^2/2C_{34}$ are introduced as frequency parameters.

The variables are quantized by the commutation relation $[\hat{\phi}_i, \hat{n}_j] = i\delta_{ij}$ as follows. \hat{n}_i is represented by $-i\partial/\partial\phi_i$ and the eigenfunction of \hat{n}_i is proportional to $e^{in_i\phi_i}$. In the basis of these eigenfunctions, we have the following matrix representation of operators:

$$\hat{n}_i = \begin{pmatrix} -N & & \\ & \ddots & \\ & & N \end{pmatrix}, \quad (\text{A5})$$

$$\cos \hat{\phi}_i = \frac{1}{2} \begin{pmatrix} & 1 & & \\ 1 & & \ddots & \\ & \ddots & & 1 \\ & & & 1 \end{pmatrix}, \quad (\text{A6})$$

$$\sin \hat{\phi}_i = \frac{1}{2i} \begin{pmatrix} & -1 & & \\ 1 & & \ddots & \\ & \ddots & & 1 \\ & & & -1 \end{pmatrix}, \quad (\text{A7})$$

where we truncate the number of Cooper pairs at $\pm N$.

Since the total system is composed of four subsystems (transmons), each operator in Eq. (A4) is represented by a tensor product of four operators, such as $\hat{n}_1 \otimes \hat{I}_2 \otimes \hat{I}_3 \otimes \hat{I}_4$, where \hat{I}_i is the identity operator for the i th subsystem of $\hat{\phi}_i$ and \hat{n}_i . From the addition theorem, $\cos(\phi_4 - \phi_3 - \Theta_{\text{ex}})$ can be expressed as $\cos \Theta_{\text{ex}} \left[\hat{I}_1 \otimes \hat{I}_2 \otimes (\cos \hat{\phi}_3 \otimes \cos \hat{\phi}_4 + \sin \hat{\phi}_3 \otimes \sin \hat{\phi}_4) \right] + \sin \Theta_{\text{ex}} \left[\hat{I}_1 \otimes \hat{I}_2 \otimes (\cos \hat{\phi}_3 \otimes \sin \hat{\phi}_4 - \sin \hat{\phi}_3 \otimes \cos \hat{\phi}_4) \right]$.

In the matrix representation, \hat{I}_i is given by the $(2N+1) \times (2N+1)$ unit matrix and the tensor product \otimes is replaced by the Kronecker product of matrices. Thus, we obtain a $(2N+1)^4 \times (2N+1)^4$ matrix representation of the Hamiltonian in Eq. (A4). In this work, we choose $N = 10$ for sufficient convergence of energies.

Numerically diagonalizing the Hamiltonian matrix with $\dot{\Phi}_{\text{ex}} = 0$, we can obtain the energies, $E_{ij,kl}$, of the state $|ij\rangle|kl\rangle$, where $|ij\rangle$ and $|kl\rangle$ denote the qubit state (qubits 1 and 2) and the coupler state (transmons 3 and 4), respectively. These energies lead to the ZZ-coupling strength ζ_{ZZ} in Figs. 2 and 3(a). For example, the energies in the case of Fig. 3 are shown in Fig. 4. The qubit energies vary a little depending on Θ_{ex} . The slopes of the qubit-energy curves give the estimated values of T_2 . Figure 4 also shows that the levels corresponding to the coupler excited states largely change by the flux and the other levels do not, as expected.

The simulation results of the CPHASE gate in Fig. 3 are obtained by numerically solving the Schrödinger equation with the Hamiltonian matrix. The average fidelity \bar{F}_{CPHASE} and the rotation angle θ_{CPHASE} of the CPHASE gate in Fig. 3 are obtained as explained in the next section.

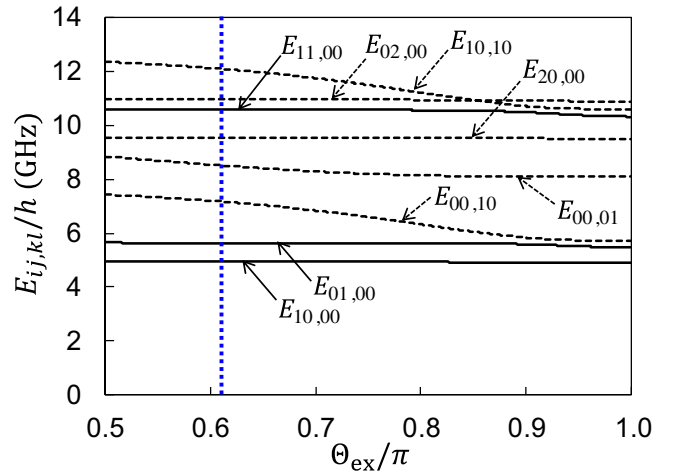


FIG. 4. The energies, $E_{ij,kl}$, of $|ij\rangle|kl\rangle$ in the case of Fig. 3 (\hbar is the Planck constant). The solid curves correspond to two-qubit states: $\omega_{ij} = E_{ij,00}/\hbar$ ($\omega_{00} = E_{00,00} = 0$). The vertical dotted line indicates the idle state ($\Theta_{\text{ex}} = 0.61\pi$).

APPENDIX B: AVERAGE FIDELITY AND ROTATION ANGLE OF THE CPHASE GATE

The average gate fidelity is a standard metric for evaluating the performance of quantum gates. It is defined by averaging gate fidelities over uniformly distributed initial states. The average fidelities in Fig. 3(d) are obtained using the formula in Ref. [76], which is an extension of the formula in Ref. [77] to cases where leakage errors exist and the norm of the qubit-subspace vector is not preserved. In the case of two-qubit gates, the formula for the average fidelity \bar{F} is given by

$$\bar{F} = \frac{|\text{tr}(U_{\text{id}}^\dagger U')|^2 + \text{tr}(U'^\dagger U')}{20}, \quad (\text{B1})$$

where U_{id} is a 4×4 unitary matrix corresponding to the ideal gate operation and U' is a 4×4 matrix defined as follows. Suppose that we simulate the gate operation on four initial states, each of which is one of the four two-qubit basis vectors denoted by $|\psi_{ij}\rangle$ ($i, j = 0, 1$). Using the resultant vectors $|\psi'_{ij}\rangle$, U' is defined as $U'_{2i+j, 2i'+j'} = \langle \psi_{ij} | \psi'_{i'j'} \rangle$. Note that U' is not a unitary matrix in general because of leakage errors. In the case of the CPHASE gate, we define U_{id} as $U_{\text{id}} = \text{diag}(e^{i\theta_0}, e^{i\theta_1}, e^{i\theta_2}, e^{i\theta_3})$, where $\text{diag}(\dots)$ represents a diagonal matrix and $e^{i\theta_k} = U'_{k,k}/|U'_{k,k}|$. By eliminating the overall phase factor and single-qubit phase rotations from U_{id} , we define the rotation angle of the CPHASE gate as $\theta_{\text{CPHASE}} = \theta_3 - \theta_1 - \theta_2 + \theta_0$.

APPENDIX C: FLUX PULSE SHAPE

As shown in Fig. 4, the higher energy levels $E_{00,10}$ and $E_{10,10}$ approach the qubit levels $E_{01,00}$ and $E_{11,00}$, respectively, around $\Theta_{\text{ex}} = \pi$. Thus, the infidelity of the CPHASE gate is mainly due to the leakage errors from $|01\rangle|00\rangle$ to $|00\rangle|10\rangle$ and from $|11\rangle|00\rangle$ to $|10\rangle|10\rangle$. To reduce these leakage errors, we design the flux pulse shape based on the technique proposed in Ref. [71]. Here, we explain how we design the pulse shape shown in Fig. 3(b).

The technique is based on the two-level system, $|g\rangle$ and $|e\rangle$, with a constant coupling rate g and a time-dependent detuning $\Delta(t)$, where the energy gap between the two energy eigenstates of this system is given by $\hbar\omega_{\text{gap}} = \hbar\sqrt{\Delta^2 + 4g^2}$. We first focus on the two levels of $|01\rangle|00\rangle$ and $|00\rangle|10\rangle$. In this case, we have $\omega_{\text{gap}} = (E_{00,10} - E_{01,00})/\hbar$ and $2g$ is given by the minimum of ω_{gap} . The energy gap is shown in Fig. 5, together with other energy gaps. From this, we obtain g and the Θ_{ex} dependencies of ω_{gap} and Δ .

The two energy eigenstates are expressed as $\cos(\theta/2)|g\rangle - \sin(\theta/2)|e\rangle$ and $\sin(\theta/2)|g\rangle + \cos(\theta/2)|e\rangle$, with $\theta = \arctan(2g/\Delta)$. Then, the nonadiabatic error probability

P_e is approximately formulated as [71]

$$P_e \approx \frac{1}{4} \left| \int_0^{T_g} \frac{d\theta}{dt} e^{-i \int_0^t \omega_{\text{gap}}(t') dt'} dt \right|^2 = \frac{1}{4} \left| \int_0^{s_f} \frac{d\theta}{ds} e^{-is} ds \right|^2, \quad (\text{C1})$$

where we introduce a dimensionless time defined as $s(t) = \int_0^t \omega_{\text{gap}}(t') dt'$ [s_f is defined as $s_f = s(T_g)$]. In this work, we set $\theta(s)$ as [71]

$$\theta(s) = \theta_0 + (\theta_1 - \theta_0) \times \frac{\left[\cos\left(2\pi \frac{s}{s_f}\right) - 1 \right] + \frac{A}{2} \left[\cos\left(4\pi \frac{s}{s_f}\right) - 1 \right]}{-2}, \quad (\text{C2})$$

where $\theta_0 = \theta(0) = \theta(s_f)$ and $\theta_1 = \theta(s_f/2)$ are θ values corresponding to $\Theta_{\text{ex}} = 0.61\pi$ and π , respectively, and the coefficient A is set as $A = -0.17$ to achieve small P_e and short T_g [78]. Using this $\theta(s)$, $t(s) = \int_0^s \omega_{\text{gap}}(s')^{-1} ds'$, and the Θ_{ex} dependencies of ω_{gap} and Δ , we obtain the corresponding pulse shape $\Theta_{\text{ex}}(t)$.

However, we find that this pulse shape leads to relatively high leakage-error probabilities from $|11\rangle|00\rangle$, though the energy gap between $|11\rangle|00\rangle$ and $|10\rangle|10\rangle$ is close to that between $|01\rangle|00\rangle$ and $|00\rangle|10\rangle$, as shown in Fig. 5. The leakage errors may be due to the smaller energy gap between $|11\rangle|00\rangle$ and $|02\rangle|00\rangle$ around $\Theta_{\text{ex}} = 0.61\pi$. Also, a slower change of Θ_{ex} around $\Theta_{\text{ex}} = \pi$ may be more desirable for increasing the rotation angle, because the ZZ-coupling strength becomes a maximum

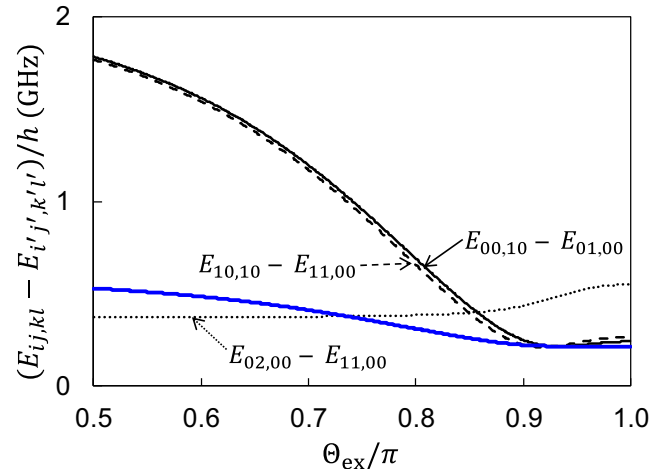


FIG. 5. Energy gaps. The thin solid curve (the energy gap between $|01\rangle|00\rangle$ and $|00\rangle|10\rangle$) is used as ω_{gap} required for designing the flux pulse shape for the CPHASE gate. The bold solid curve (in blue), which is given by Eq. (C3), is used as ω_{gap} in $t(s) = \int_0^s \omega_{\text{gap}}(s')^{-1} ds'$.

there. Inspired by this, we modify the energy gap used for $t(s) = \int_0^s \omega_{\text{gap}}(s')^{-1} ds'$ as

$$\begin{cases} 0.2[(E_{00,10} - E_{01,00})/\hbar - 2g] + 2g & \dots & \Theta_{\text{ex}} \leq \Theta_{\text{ex}}^{(g)}, \\ 2g & \dots & \Theta_{\text{ex}} > \Theta_{\text{ex}}^{(g)}, \end{cases} \quad (\text{C3})$$

which is shown by the bold solid curve (in blue) in Fig. 5 [$\Theta_{\text{ex}}^{(g)}$ is Θ_{ex} satisfying $(E_{00,10} - E_{01,00})/\hbar = 2g$]. Thus, we obtain the pulse shape shown in Fig. 3(b).

APPENDIX D: PARAMETER VALUES IN NUMERICAL STUDIES

The parameter values used for the present numerical studies are set as follows. Note that the present system can be regarded as a network of capacitively coupled four transmons, except for the interaction between transmons 3 and 4 through the additional Josephson junction given by the last term in Eq. (4). The transmon network is quantized by the standard method using bosonic operators [79]. Its Hamiltonian is given by

$$\hat{H}' = \sum_{i=1}^4 \left(\hbar \omega_i \hat{a}_i^\dagger \hat{a}_i - \hbar \frac{W_{ii}}{2} \hat{a}_i^{\dagger 2} \hat{a}_i^2 \right) + \sum_{i=1}^3 \sum_{j=i+1}^4 \hbar g_{ij} (\hat{a}_i^\dagger \hat{a}_j + \hat{a}_j^\dagger \hat{a}_i), \quad (\text{D1})$$

TABLE I. The parameter settings for the present numerical studies. The bold values are design values. The others are calculated from their definitions using the design values.

$\omega_1/(2\pi)$ (GHz)	5	$W_{11}/(2\pi)$ (MHz)	296
$\omega_2/(2\pi)$ (GHz)	5.7	$W_{12}/(2\pi)$ (MHz)	0.19
$\omega_3/(2\pi)$ (GHz)	7.2	$W_{13}/(2\pi)$ (MHz)	26.5
$\omega_4/(2\pi)$ (GHz)	8.5	$W_{14}/(2\pi)$ (MHz)	0.63
C_{11} (fF)	60	$W_{22}/(2\pi)$ (MHz)	296
C_{12} (fF)	0.025	$W_{23}/(2\pi)$ (MHz)	0.63
C_{13} (fF)	6	$W_{24}/(2\pi)$ (MHz)	26.5
C_{14} (fF)	0.05	$W_{33}/(2\pi)$ (MHz)	291
C_{22} (fF)	60	$W_{34}/(2\pi)$ (MHz)	4.42
C_{23} (fF)	0.05	$W_{44}/(2\pi)$ (MHz)	291
C_{24} (fF)	6	$\omega_{J1}/(2\pi)$ (GHz)	11.9
C_{33} (fF)	60	$\omega_{J2}/(2\pi)$ (GHz)	15.2
C_{34} (fF)	1	$\omega_{J3}/(2\pi)$ (GHz)	24.1
C_{44} (fF)	60	$\omega_{J4}/(2\pi)$ (GHz)	33.2
$g_{12}/(2\pi)$ (MHz)	1.7	$\omega_{J5}/(2\pi)$ (GHz)	7.2
$g_{13}/(2\pi)$ (MHz)	239	$I_{c1}/(2\pi)$ (nA)	23.9
$g_{14}/(2\pi)$ (MHz)	5.7	$I_{c2}/(2\pi)$ (nA)	30.6
$g_{23}/(2\pi)$ (MHz)	6.5	$I_{c3}/(2\pi)$ (nA)	48.5
$g_{24}/(2\pi)$ (MHz)	270	$I_{c4}/(2\pi)$ (nA)	66.8
$g_{34}/(2\pi)$ (MHz)	57	$I_{c5}/(2\pi)$ (nA)	14.4

$$\omega_i = \sqrt{8W_{ii}\omega_{Ji}} - W_{ii}, \quad (\text{D2})$$

$$g_{ij} = \frac{W_{ij}}{2} \sqrt{\frac{(\omega_i + W_{ii})(\omega_j + W_{jj})}{W_{ii}W_{jj}}}, \quad (\text{D3})$$

where \hat{a}_i and \hat{a}_i^\dagger are the annihilation and creation operators, respectively, for the i th transmon. In this work, we set the transmon frequencies ω_i and capacitances as design values, as given in Fig. 2. The parasitic capacitances not shown in Fig. 1 are ideally set to zero but this is impossible in actual experiments. Among the parasitic capacitances, C_{34} is set to a relatively large value, because transmons 3 and 4 are directly coupled via the Josephson junction with the critical current of I_{c5} . On the other hand, the other parasitic capacitances, which comprise nonadjacent transmons, are set to small values, which may be feasible by placing the nonadjacent transmons as far from each other as possible. The other parameters are determined by their definitions, together with $\omega_{J5} = (\omega_{J3} + \omega_{J4})/8$ (a quarter of the mean value of ω_{J3} and ω_{J4}). Table I summarizes the design values (shown in bold) and resultant other parameter values used in this work. The anharmonicities (Kerr coefficients) of the transmons are given by W_{ii} , which are about 0.3 GHz.

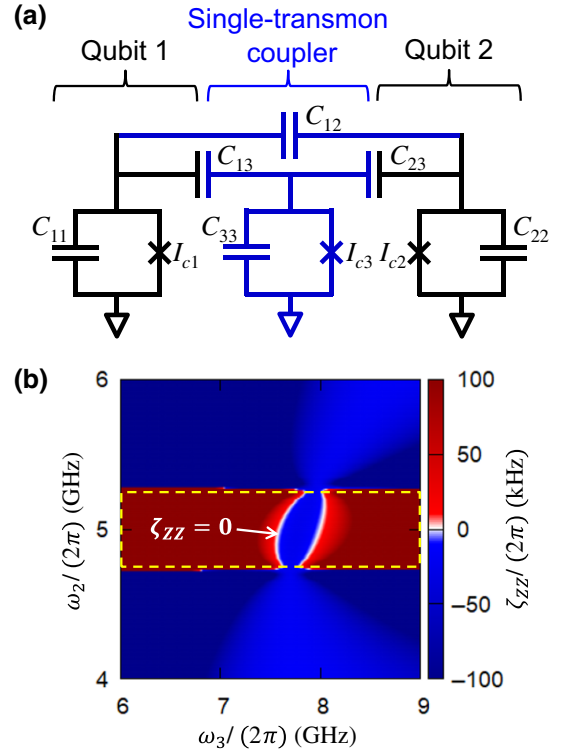


FIG. 6. The single-transmon coupler. (a) A simplified diagram. (b) The ZZ-coupling strength ζ_{ZZ} with $\omega_1/(2\pi) = 5$ GHz, $W_{11}/(2\pi) = W_{22}/(2\pi) = W_{33}/(2\pi) = 250$ MHz, $g_{13}/(2\pi) = g_{23}/(2\pi) = 250$ MHz, and $g_{12}/(2\pi) = 25$ MHz. The dashed yellow box indicates the region in the straddling regime.

APPENDIX E: SINGLE-TRANSMON COUPLER

The conventional single-transmon coupler is shown in Fig. 6(a), in which the dc superconducting quantum interference device (SQUID) for the frequency-tunable transmon in the coupler is replaced by a single Josephson junction for simplicity. Figure 6(b) shows the ZZ-coupling strength, ζ_{ZZ} , of the coupler with typical parameter values [43]. Note that ZZ-coupling vanishing points [the white region in Fig. 6(b)] exist only in the straddling regime [the dashed yellow box in Fig. 6(b)]. Thus, the single-transmon coupler cannot realize zero ZZ coupling for highly detuned qubits. This is a vital contrast to the proposed double-transmon coupler.

-
- [1] D. Deutsch, A. Barenco, and A. Ekert, Universality in quantum computation, *Proc. R. Soc. Lond. A* **449**, 669 (1995).
 - [2] A. Barenco, A universal two-bit gate for quantum computation, *Proc. R. Soc. Lond. A* **449**, 679 (1995).
 - [3] D. P. DiVincenzo, Two-bit gates are universal for quantum computation, *Phys. Rev. A* **51**, 1015 (1995).
 - [4] T. Sleator and H. Weinfurter, Realizable Universal Quantum Logic Gates, *Phys. Rev. Lett.* **74**, 4087 (1995).
 - [5] S. Lloyd, Almost Any Quantum Logic Gate is Universal, *Phys. Rev. Lett.* **75**, 346 (1995).
 - [6] A. Barenco, C. H. Bennett, R. Cleve, D. P. DiVincenzo, N. Margolus, P. Shor, T. Sleator, J. A. Smolin, and H. Weinfurter, Elementary gates for quantum computation, *Phys. Rev. A* **52**, 3457 (1995).
 - [7] M. A. Nielsen and I. L. Chuang, *Quantum Computation and Quantum Information* (Cambridge University Press, Cambridge, England, 2000).
 - [8] R. Raussendorf and J. Harrington, Fault-Tolerant Quantum Computation with High Threshold in Two Dimensions, *Phys. Rev. Lett.* **98**, 190504 (2007).
 - [9] R. Raussendorf, J. Harrington, and K. Goyal, Topological fault-tolerance in cluster state quantum computation, *New J. Phys.* **9**, 199 (2007).
 - [10] A. G. Fowler, A. M. Stephens, and P. Groszkowski, High-threshold universal quantum computation on the surface code, *Phys. Rev. A* **80**, 052312 (2009).
 - [11] D. S. Wang, A. G. Fowler, and L. C. L. Hollenberg, Surface code quantum computing with error rates over 1%, *Phys. Rev. A* **83**, 020302(R) (2011).
 - [12] A. G. Fowler, M. Mariantoni, J. M. Martinis, and A. N. Cleland, Surface codes: Towards practical large-scale quantum computation, *Phys. Rev. A* **86**, 032324 (2012).
 - [13] C. J. Ballance, T. P. Harty, N. M. Linke, M. A. Sepiol, and D. M. Lucas, High-Fidelity Quantum Logic Gates Using Trapped-Ion Hyperfine Qubits, *Phys. Rev. Lett.* **117**, 060504 (2016).
 - [14] J. P. Gaebler, T. R. Tan, Y. Lin, Y. Wan, R. Bowler, A. C. Keith, S. Glancy, K. Coakley, E. Knill, D. Leibfried, and D. J. Wineland, High-Fidelity Universal Gate Set for $^9\text{Be}^+$ Ion Qubits, *Phys. Rev. Lett.* **117**, 060505 (2016).
 - [15] V. M. Schäfer, C. J. Ballance, K. Thirumalai, L. J. Stephenson, T. G. Ballance, A. M. Steane, and D. M. Lucas, Fast quantum logic gates with trapped-ion qubits, *Nature* **555**, 75 (2018).
 - [16] J. M. Pino, J. M. Dreiling, C. Figgatt, J. P. Gaebler, S. A. Moses, M. S. Allman, C. H. Baldwin, M. Foss-Feig, D. Hayes, K. Mayer, C. Ryan-Anderson, and B. Neyenhuis, Demonstration of the trapped-ion quantum CCD computer architecture, *Nature* **592**, 209 (2021).
 - [17] L. Egan, D. M. Debroy, C. Noel, A. Risinger, D. Zhu, D. Biswas, M. Newman, M. Li, K. R. Brown, M. Cetina, and C. Monroe, Fault-tolerant control of an error-corrected qubit, *Nature* **598**, 281 (2021).
 - [18] C. Ryan-Anderson, J. G. Bohnet, K. Lee, D. Gresh, A. Hankin, J. P. Gaebler, D. Francois, A. Chernoguzov, D. Lucchetti, N. C. Brown, T. M. Gatterman, S. K. Halit, K. Gilmore, J. A. Gerber, B. Neyenhuis, D. Hayes, and R. P. Stutz, Realization of real-time fault-tolerant quantum error correction, *Phys. Rev. X* **11**, 041058 (2021).
 - [19] R. Barends *et al.*, Superconducting quantum circuits at the surface code threshold for fault tolerance, *Nature* **508**, 500 (2014).
 - [20] J. Kelly *et al.*, State preservation by repetitive error detection in a superconducting quantum circuit, *Nature* **519**, 66 (2015).
 - [21] F. Arute *et al.*, Quantum supremacy using a programmable superconducting processor, *Nature* **574**, 505 (2019).
 - [22] B. Foxen *et al.*, Demonstrating a Continuous Set of Two-Qubit Gates for Near-Term Quantum Algorithms, *Phys. Rev. Lett.* **125**, 120504 (2020).
 - [23] Y. Xu, J. Chu, J. Yuan, J. Qiu, Y. Zhou, L. Zhang, X. Tan, Y. Yu, S. Liu, J. Li, F. Yan, and D. Yu, High-Fidelity, High-Scalability Two-Qubit Gate Scheme for Superconducting Qubits, *Phys. Rev. Lett.* **125**, 240503 (2020).
 - [24] Y. Wu *et al.*, Strong Quantum Computational Advantage Using a Superconducting Quantum Processor, *Phys. Rev. Lett.* **127**, 180501 (2021).
 - [25] Q. Ficheux, L. B. Nguyen, A. Somoroff, H. Xiong, K. N. Nesterov, M. G. Vavilov, and V. E. Manucharyan, Fast logic with slow qubits: Microwave-activated controlled-Z gate on low-frequency fluxoniums, *Phys. Rev. X* **11**, 021026 (2021).
 - [26] V. Negîrneac, H. Ali, N. Muthusubramanian, F. Battistel, R. Sagastizabal, M. S. Moreira, J. F. Marques, W. J. Vlothuizen, M. Beekman, C. Zachariadis, N. Haider, A. Bruno, and L. DiCarlo, High-Fidelity Controlled-Z Gate with Maximal Intermediate Leakage Operating at the Speed Limit in a Superconducting Quantum Processor, *Phys. Rev. Lett.* **126**, 220502 (2021).
 - [27] Y. Sung, L. Ding, J. Braumüller, A. Vepsäläinen, B. Kannan, M. Kjaergaard, A. Greene, G. O. Samach, C. McNally, D. Kim, A. Melville, B. M. Niedzielski, M. E. Schwartz, J. L. Yoder, T. P. Orlando, S. Gustavsson, and W. D. Oliver, Realization of high-fidelity CZ and ZZ-free *i*SWAP gates with a tunable coupler, *Phys. Rev. X* **11**, 021058 (2021).
 - [28] J. Stehlik, D. M. Zajac, D. L. Underwood, T. Phung, J. Blair, S. Carnevale, D. Klaus, G. A. Keefe, A. Carniol, M. Kumph, M. Steffen, and O. E. Dial, Tunable Coupling Architecture for Fixed-Frequency Transmon Superconducting Qubits, *Phys. Rev. Lett.* **127**, 080505 (2021).

- [29] E. A. Sete, N. Didier, A. Q. Chen, S. Kulshreshtha, R. Manenti, and S. Poletto, Parametric-Resonance Entangling Gates with a Tunable Coupler, *Phys. Rev. Appl.* **16**, 024050 (2021).
- [30] A. Kandala, K. X. Wei, S. Srinivasan, E. Magesan, S. Carnevale, G. A. Keefe, D. Klaus, O. Dial, and D. C. McKay, Demonstration of a High-Fidelity CNOT Gate for Fixed-Frequency Transmons with Engineered ZZ Suppression, *Phys. Rev. Lett.* **127**, 130501 (2021).
- [31] B. K. Mitchell, R. K. Naik, A. Morvan, A. Hashim, J. M. Kreikebaum, B. Marinelli, W. Lavrijsen, K. Nowrouzi, D. I. Santiago, and I. Siddiqi, Hardware-Efficient Microwave-Activated Tunable Coupling between Superconducting Qubits, *Phys. Rev. Lett.* **127**, 200502 (2021).
- [32] Y. Ye *et al.*, Realization of high-fidelity CZ gates in extensible superconducting qubits design with a tunable coupler, [arXiv:2109.05680](https://arxiv.org/abs/2109.05680).
- [33] A. Noiri, K. Takeda, T. Nakajima, T. Kobayashi, A. Sammak, G. Scappucci, and S. Tarucha, Fast universal quantum gate above the fault-tolerance threshold in silicon, *Nature* **601**, 338 (2022).
- [34] X. Xue, M. Russ, N. Samkharadze, B. Undseth, A. Sammak, G. Scappucci, and L. M. K. Vandersypen, Quantum logic with spin qubits crossing the surface code threshold, *Nature* **601**, 343 (2022).
- [35] A. R. Mills, Charles R. Guinn, M. J. Gullans, A. J. Sigillito, M. M. Feldman, E. Nielsen, and J. R. Petta, Two-qubit silicon quantum processor with operation fidelity exceeding 99%, *Sci. Adv.* **8**, eabn5130 (2022).
- [36] M. T. Mądzik, S. Asaad, A. Youssry, B. Joecker, K. M. Rudinger, E. Nielsen, K. C. Young, T. J. Proctor, A. D. Baczewski, A. Laucht, V. Schmitt, F. E. Hudson, K. M. Itoh, A. M. Jakob, B. C. Johnson, D. N. Jamieson, A. S. Dzurak, C. Ferrie, R. Blume-Kohout, and A. Morello, Precision tomography of a three-qubit donor quantum processor in silicon, *Nature* **601**, 348 (2022).
- [37] M. Gong *et al.*, Quantum walks on a programmable two-dimensional 62-qubit superconducting processor, *Science* **372**, 948 (2021).
- [38] D. R. W. Yost, M. E. Schwartz, J. Mallek, D. Rosenberg, C. Stull, J. L. Yoder, G. Calusine, M. Cook, R. Das, A. L. Day, E. B. Golden, D. K. Kim, A. Melville, B. M. Niedzielski, W. Woods, A. J. Kerman, and W. D. Oliver, Solid-state qubits integrated with superconducting through-silicon vias, *npj Quant. Inf.* **6**, 59 (2020).
- [39] J. L. Mallek, D.-R. W. Yost, D. Rosenberg, J. L. Yoder, G. Calusine, M. Cook, R. Das, A. Day, E. Golden, D. K. Kim, J. Knecht, B. M. Niedzielski, M. Schwartz, A. Sevi, C. Stull, W. Woods, A. J. Kerman, and W. D. Oliver, Fabrication of superconducting through-silicon vias, [arXiv:2103.08536](https://arxiv.org/abs/2103.08536).
- [40] S. Kosen *et al.*, Building blocks of a flip-chip integrated superconducting quantum processor, [arXiv:2112.02717](https://arxiv.org/abs/2112.02717).
- [41] P. Mundada, G. Zhang, T. Hazard, and A. Houck, Suppression of Qubit Crosstalk in a Tunable Coupling Superconducting Circuit, *Phys. Rev. Appl.* **12**, 054023 (2019).
- [42] X. Li, T. Cai, H. Yan, Z. Wang, X. Pan, Y. Ma, W. Cai, J. Han, Z. Hua, X. Han, Y. Wu, H. Zhang, H. Wang, Y. Song, L. Duan, and L. Sun, Tunable Coupler for Realizing a Controlled-Phase Gate with Dynamically Decoupled Regime in a Superconducting Circuit, *Phys. Rev. Appl.* **14**, 024070 (2020).
- [43] M. C. Collodo, J. Herrmann, N. Lacroix, C. K. Andersen, A. Remm, S. Lazar, J.-C. Besse, T. Walter, A. Wallraff, and C. Eichler, Implementation of Conditional Phase Gates Based on Tunable ZZ Interactions, *Phys. Rev. Lett.* **125**, 240502 (2020).
- [44] Z. Ni, S. Li, L. Zhang, J. Chu, J. Niu, T. Yan, X. Deng, L. Hu, J. Li, Y. Zhong, S. Liu, F. Yan, Y. Xu, and D. Yu, Scalable method for eliminating residual ZZ interaction between superconducting qubits, [arXiv:2111.13292](https://arxiv.org/abs/2111.13292).
- [45] A. Petrescu, C. L. Calonnec, C. Leroux, A. D. Paolo, P. Mundada, S. Sussman, A. Vrajitoarea, A. A. Houck, and A. Blais, Accurate methods for the analysis of strong-drive effects in parametric gates, [arXiv:2107.02343](https://arxiv.org/abs/2107.02343).
- [46] L. Jin, Implementing high-fidelity two-qubit gates in superconducting coupler architecture with novel parameter regions, [arXiv:2105.13306](https://arxiv.org/abs/2105.13306).
- [47] C. Leroux, A. D. Paolo, and A. Blais, Superconducting Coupler with Exponentially Large On/Off Ratio, *Phys. Rev. Appl.* **16**, 064062 (2021).
- [48] T. Miyanaga, A. Tomonaga, H. Ito, H. Mukai, and J. S. Tsai, Ultrastrong Tunable Coupler Between Superconducting LC Resonators, *Phys. Rev. Appl.* **16**, 064041 (2021).
- [49] P. Krantz, M. Kjaergaard, F. Yan, T. P. Orlando, S. Gustavsson, and W. D. Oliver, A quantum engineer's guide to superconducting qubits, *Appl. Phys. Rev.* **6**, 021318 (2019).
- [50] F. Yan, P. Krantz, Y. Sung, M. Kjaergaard, D. L. Campbell, T. P. Orlando, S. Gustavsson, and W. D. Oliver, Tunable Coupling Scheme for Implementing High-Fidelity Two-Qubit Gates, *Phys. Rev. Appl.* **10**, 054062 (2018).
- [51] A. O. Niskanen, Y. Nakamura, and J.-S. Tsai, Tunable coupling scheme for flux qubits at the optimal point, *Phys. Rev. B* **73**, 094506 (2006).
- [52] A. O. Niskanen, K. Harrabi, F. Yoshihara, Y. Nakamura, S. Lloyd, and J. S. Tsai, Quantum coherent tunable coupling of superconducting qubits, *Science* **316**, 723 (2007).
- [53] M. S. Allman, J. D. Whittaker, M. Castellanos-Beltran, K. Cicak, F. da Silva, M. P. DeFeo, F. Lecocq, A. Sirois, J. D. Teufel, J. Aumentado, and R. W. Simmonds, Tunable Resonant and Nonresonant Interactions between a Phase Qubit and LC Resonator, *Phys. Rev. Lett.* **112**, 123601 (2014).
- [54] J. D. Whittaker, F. C. S. da Silva, M. S. Allman, F. Lecocq, K. Cicak, A. J. Sirois, J. D. Teufel, J. Aumentado, and R. W. Simmonds, Tunable-cavity QED with phase qubits, *Phys. Rev. B* **90**, 024513 (2014).
- [55] Y. Chen *et al.*, Qubit Architecture with High Coherence and Fast Tunable Coupling, *Phys. Rev. Lett.* **113**, 220502 (2014).
- [56] C. Neill *et al.*, A blueprint for demonstrating quantum supremacy with superconducting qubits, *Science* **360**, 195 (2018).
- [57] P. Zhao, P. Xu, D. Lan, J. Chu, X. Tan, H. Yu, and Y. Yu, High-Contrast ZZ Interaction Using Superconducting Qubits with Opposite-Sign Anharmonicity, *Phys. Rev. Lett.* **125**, 200503 (2020).
- [58] J. Ku, X. Xu, M. Brink, D. C. McKay, J. B. Hertzberg, M. H. Ansari, and B. L. T. Plourde, Suppression of Unwanted ZZ Interactions in a Hybrid Two-Qubit System, *Phys. Rev. Lett.* **125**, 200504 (2020).

- [59] A. Noguchi, A. Osada, S. Masuda, S. Kono, K. Heya, S. P. Wolski, H. Takahashi, T. Sugiyama, D. Lachance-Quirion, and Y. Nakamura, Fast parametric two-qubit gates with suppressed residual interaction using the second-order non-linearity of a cubic transmon, *Phys. Rev. A* **102**, 062408 (2020).
- [60] X. Xu and M. H. Ansari, ZZ Freedom in Two-Qubit Gates, *Phys. Rev. Appl.* **15**, 064074 (2021).
- [61] P. Zhao, D. Lan, P. Xu, G. Xue, M. Blank, X. Tan, H. Yu, and Y. Yu, Suppression of Static ZZ Interaction in an All-Transmon Quantum Processor, *Phys. Rev. Appl.* **16**, 024037 (2021).
- [62] A. D. K. Finck, S. Carnevale, D. Klaus, C. Scerbo, J. Blair, T. G. McConkey, C. Kurter, A. Carniol, G. Keefe, M. Kumph, and O. E. Dial, Suppressed Crosstalk between Two-Junction Superconducting Qubits with Mode-Selective Exchange Coupling, *Phys. Rev. Appl.* **16**, 054041 (2021).
- [63] V. Tripathi, H. Chen, M. Khezri, K.-W. Yip, E. M. Levenson-Falk, and D. A. Lidar, Suppression of crosstalk in superconducting qubits using dynamical decoupling, *arXiv:2108.04530*.
- [64] Recently, couplers with a flux qubit, instead of a frequency-tunable transmon, have been proposed [45,46]. These use three or more Josephson junctions, like our double-transmon coupler. However, they are rather similar to the single-transmon coupler and notably different from the double-transmon coupler.
- [65] This qualitative and classical explanation under rough approximations describes how we find the concept of the double-transmon coupler. While this will be helpful for intuitive understanding of the mechanism, we must investigate the coupler in a more accurate manner to evaluate its performance, which is presented later.
- [66] \hbar and $\phi_0 = \Phi_0/(2\pi)$ are, respectively, the reduced Planck constant and the reduced flux quantum (Φ_0 is the flux quantum).
- [67] This holds when the loop self-inductance is negligible.
- [68] J. Koch, T. M. Yu, J. Gambetta, A. A. Houck, D. I. Schuster, J. Majer, A. Blais, M. H. Devoret, S. M. Girvin, and R. J. Schoelkopf, Charge-insensitive qubit design derived from the Cooper pair box, *Phys. Rev. A* **76**, 042319 (2007).
- [69] We find this fact by numerical studies. Its theoretical explanation is desirable but is left for future work.
- [70] We choose the parameters in Fig. 2(a) (out of the straddling regime), because in this work, we are interested in highly detuned qubits. We also choose $\omega_4/(2\pi) = 8.5$ GHz as a relatively low value among the values satisfying the zero ZZ coupling. [We avoid the lower-bound value (about 8.3 GHz), because this may be not robust against small errors in parameter values.].
- [71] J. M. Martinis and M. R. Geller, Fast adiabatic qubit gates using only σ_z control, *Phys. Rev. A* **90**, 022307 (2014).
- [72] When there are more qubits, gate operations on other qubits will affect the performance; in particular, the zero ZZ coupling. This is an important issue but its simulation calls for massive computations. Therefore, the study of this issue is left for future work.
- [73] A. P. M. Place *et al.*, New material platform for superconducting transmon qubits with coherence times exceeding 0.3 milliseconds, *Nat. Commun.* **12**, 1779 (2021).
- [74] C. Wang *et al.*, Towards practical quantum computers: Transmon qubit with a lifetime approaching 0.5 milliseconds, *npj Quantum Inf.* **8**, 3 (2022).
- [75] J. B. Hertzberg, E. J. Zhang, S. Rosenblatt, E. Magesan, J. A. Smolin, J.-B. Yau, V. P. Adiga, M. Sandberg, M. Brink, J. M. Chow, and J. S. Orcutt, Laser-annealing Josephson junctions for yielding scaled-up superconducting quantum processors, *npj Quantum Inf.* **7**, 129 (2021).
- [76] R. Kueng, D. M. Long, A. C. Doherty, and S. T. Flammia, Comparing Experiments to the Fault-Tolerance Threshold, *Phys. Rev. Lett.* **117**, 170502 (2016).
- [77] M. A. Nielsen, A simple formula for the average gate fidelity of a quantum dynamical operation, *Phys. Lett. A* **303**, 249 (2002).
- [78] This value is chosen by trial and error.
- [79] A. Blais, A. L. Grimsmo, S. M. Girvin, and A. Wallraff, Circuit quantum electrodynamics, *Rev. Mod. Phys.* **93**, 025005 (2021).